Soils and Foundations 2012;52(4):737–747

The Japanese Geotechnical Society

Soils and Foundations

www.sciencedirect.com
journal homepage: www.elsevier.com/locate/sandf

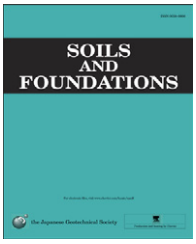

Stability monitoring of rainfall-induced deep landslides through pore pressure profile measurements

An-Bin Huang[a,1], Jui-Ting Lee[a,*], Yen-Te Ho[a,2], Yun-Fang Chiu[b,3], Shyr-Yuan Cheng[c,4]

[a]*Department of Civil Engineering, National Chiao-Tung University, Hsinchu, Taiwan*
[b]*Harbor and Marine Technology Center, Taichung, Taiwan*
[c]*Telecommunication Labs, Chunghwa Telecom Co., Taoyuan, Taiwan*

Received 14 December 2011; received in revised form 25 April 2012; accepted 20 June 2012
Available online 7 September 2012

Abstract

It has long been recognized that field hydrological and geomechanical properties/conditions are the key elements controlling the stability of a slope under the influence of rainfall. Warning systems based on rainfall or ground displacement measurements are popular methods currently being used to minimize the hazards of landslides. When field hydrological monitoring is used, it usually involves a limited number of sensors for either positive or negative pore-water pressure measurements. The available numerical schemes that couple pore-water pressure with a geomechanical analysis are the most suitable for shallow slope failures. Due to the variable and transient nature of the hydrological conditions in earth slopes, field measurements that reflect the pore-water pressure profile on a real-time basis would be highly desirable. Thus, the authors have developed a piezometer system that is based on optical fiber Bragg grating (FBG) pressure sensors. With this system, an array of nine sensors was installed in a single, 60-m-deep borehole to monitor the pore-water pressure profile in a highway slope in Southern Taiwan. This paper describes the details of the FBG sensor array installation in the field and the data obtained throughout three typhoons from 2008 to 2010. The results demonstrate that the field readings can be readily incorporated into the existing mechanics-based analytical framework and can predict the potential of an upcoming slope failure.

Keywords: Fiber optic sensing; Pore-water pressure; Landslide; Rainfall

1. Introduction

Rainfall has been considered as one of the most frequent triggering factors to natural slope failures (De Vita and Reichenbach, 1998). Keefer et al. (1987) described a real-time landslide warning system based primarily on the precipitation intensity-duration thresholds developed by Cannon and Ellen (1985), with consideration also given to seasonal antecedent precipitation. Rainfall intensity-duration threshold-based methods are empirically developed using previous records for a given region.

It has long been recognized that field hydrological and geomechanical properties/conditions are the key elements controlling the stability of a slope under the influence of

*Corresponding author. Tel.: +886 35712121x55009; fax: +886 35716257.
E-mail addresses: abhuang@mail.nctu.edu.tw (A.-B. Huang), ruiting.cv92g@nctu.edu.tw (J.-T. Lee), ytho@mail.nctu.edu.tw (Y.-T. Ho), yfchiu@mail.ihmt.gov.tw (Y.-F. Chiu). st@cht.com.tw (S.-Y. Cheng).
[1]Tel.: +886 722803; fax: +886 35716257.
[2]Tel.: +886 35712121x55270; fax: +886 35716257.
[3]Tel.: +886 426587200; fax: +886 426571329.
[4]Tel.: +886 34244345; fax: +886 34244099.
Peer review under responsibility of The Japanese Geotechnical Society.

0038-0806
http://dx.doi.org/10.1016/j.sandf.2012.07.013

rainfall (Johnson and Sitar, 1990; Anderson and Sitar, 1995; Fannin and Jaakkola, 1999; Collins and Znidarcic, 2004; Cascini et al., 2010; Kitamura and Sako, 2010; Rahardjo et al., 2010). Thus, a mechanics-based system that considers the current and local soil/groundwater conditions should be a desirable approach to providing an effective analysis or warning for a potential landslide at a given location.

Collins and Znidarcic (2004) analyzed shallow landslides with failure planes that have small depth-to-length ratios, as infinitely long slope failures. It was assumed that each slice of the infinitely long slope was subjected to a uniform rainfall event. An individual slice was numerically simulated as a one-dimensional soil column subjected to vertical infiltration. The one-dimensional seepage analysis computes the transient capillary and pore-water pressure head (h_c and h_p, respectively) profiles in response to rainfall water infiltration. For slopes with a low groundwater table, the soil is initially unsaturated. The downward infiltration progressively increases the degree of saturation in the soil with depth. For coarse-grained soils, the hydraulic conductivity increases significantly with the degree of saturation. Thus, pore-water pressure tends to accumulate in coarse-grained soil situations as water infiltrates from the more saturated surficial soil into the deeper, less saturated soil with lower permeability. The development of positive pore pressure is analogous to the establishment of a perched water table in the upper part of the layer. For fine-grained soils, such high gradients are absent from the infiltration profiles, since the hydraulic conductivity changes more gradually.

Considering the equilibrium of gravity, the available soil resistance and the seepage forces imposing on the slice, the relationship among the critical depth for the infinite slope failure (d_{cr}), the soil strength parameters and the pore-water pressure head was established as

$$\frac{d_{cr}=c'+\gamma_w\cdot h_c\cdot\tan\phi^b-\gamma_w\cdot h_p\cdot\tan\phi'}{\gamma\cdot\cos^2\beta\cdot(\tan\beta-\tan\phi')} \quad (1)$$

where β, slope angle; c', drained cohesion; γ, saturated unit weight of soil; γ_w, unit weight of water; ϕ', drained friction angle; ϕ^b, friction angle with respect to matric suction ($=\gamma_w h_c$).

In unsaturated soil, $h_p=0$, and when the soil becomes saturated, $h_c=0$. According to Eq. (1), for slope angles less than the friction angle ($\beta<\phi'$), failure in the unsaturated soil layer is not possible. In the case of $\beta>\phi'$, the slope can fail when the soil is still unsaturated with negative pore-water pressure. The coupling of Eq. (1) and the one-dimensional seepage analysis enables quantitative predictions of the time and the depth of a shallow slope failure. Fig. 1 shows the results for a fictitious case of $\beta<\phi'$, with a coarse-grained soil, reported by Collins and Znidarcic (2004). The pressure head profiles (h_c or h_p versus depth of infiltration) evolve as the infiltration progresses in a rainfall event. Slope failure occurs at depth d_{cr}, where the pressure head profile touches the stability envelope.

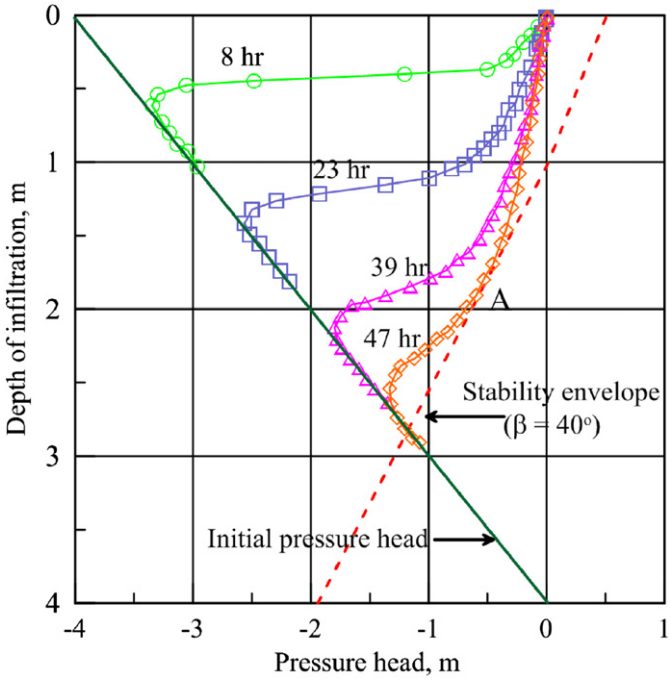

Fig. 1. Infiltration results for a fictitious case of $\beta<\phi'$ or coarse-grained soil with superimposed stability envelope (after Collins and Znidarcic, 2004).

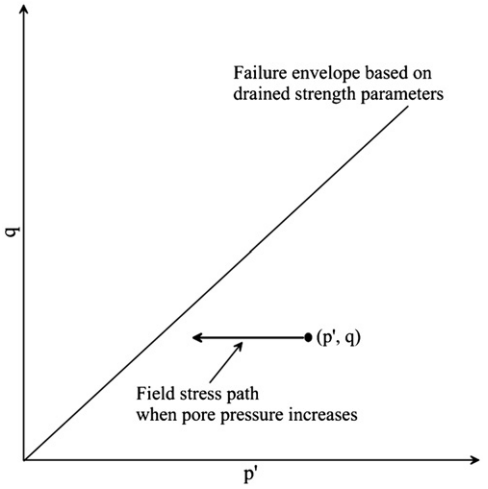

Fig. 2. Field stress path.

The stability envelope is a graphic presentation of Eq. (1). Researchers have also used the concept of field stress paths to describe the changes in stress from the hydrological response (Anderson and Sitar, 1995; Cascini et al., 2010). For given strength parameters or the failure envelope of the slope soil, the initial effective stress points (p', q) of the soil within a stable slope are located at the right side of the drained failure envelope, as qualitatively described in Fig. 2. The definitions for p' and q to be used in this paper are

$$p'=(\sigma_1'+\sigma_2'+\sigma_3')/3 \quad (2)$$

$$q=\frac{1}{\sqrt{2}}\sqrt{(\sigma_1'-\sigma_3')^2+(\sigma_1'-\sigma_2')^2+(\sigma_2'-\sigma_3')^2} \quad (3)$$

where σ_1', σ_2' and σ_3' is the major, intermediate and minor principal stress, respectively.

Changes in soil saturation and seepage direction, as a result of water infiltration, can affect the shear stress. However, these effects are believed to be insignificant, and the stress points (p', q) generally move in the horizontal direction as the field pore water increases.

Pore-water pressure is probably the most indicative of slope instability in its early stage, among the viable physical quantities that can be monitored in the field. The monitoring of positive and negative pore pressure, using piezometers and tensiometers, respectively, has been reported for slopes in different parts of the world (Cowland and Richards, 1985; Johnson and Sitar, 1990; Fannin and Jaakkola, 1999; Ng et al., 2003, 2008; Zhan et al., 2007). In general, a tensiometer is directly inserted into a shallow ground to measure the negative pore pressure at a single depth. The current practice at groundwater level or for positive pore-water pressure monitoring usually involves the installation of one or two open end piezometers (i.e., standpipes) and pneumatic or electric pressure transducers in a typical 100 mm-diameter borehole. Fannin and Jaakkola (1999) reported from their experiences that the field pore pressure measurements rarely showed a linear distribution with depth or a uniform response across the slope. Soil stratification and subsurface conduits, such as soil pipes or animal burrows, create highly permeable drainage paths (Johnson and Sitar, 1990; Fannin and Jaakkola, 1999). When blocked, these conditions can create instant pore pressure buildup. Sidle (1984) has also indicated that pore pressure buildup can occur quite rapidly, can vary in character along the slope and cannot be entirely explained by assuming only vertical infiltration through the soil.

Due to their geological and meteorological conditions, landslides during typhoon season are common in Taiwan. A relatively deep and massive landslide occurred above Shiaolin Village of Kaohsiung County in Taiwan during typhoon Morakot of 2009. The debris buried and killed 500 local residents. The slope angle before failure was less than 23° and the failure surface was approximately 84 m deep. Deep-seated slope failures are relatively rare, but their consequences can be devastating. An effective landslide warning system would be very useful for mitigating the hazards of such deep-seated and potentially massive landslides.

The above-described literature often referred to their analyses as "shallow" slope failures, with depths of shear planes generally less than 5 m. For deep-seated landslides, the direct measurement of the pore-water pressure profile on a real-time basis would be desirable. The field monitoring should be automated and have sufficient measurement points to reveal the highly non-linear and transient pore-water pressure profiles resulting from heavy rainfall. There are commercially available vibrating wire (VW) piezometers that allow multiple units to be connected in a series and installed in a single borehole. Electric sensors, such as the VW piezometers, can be affected by electromagnetic interference, lightning and/or short circuits when placed under water in the field. Little has been reported on the long term, automated pore-water pressure profile monitoring using an array of the VW type of piezometers.

Fiber Bragg grating (FBG) is a partially distributive optical fiber sensor whereby the signal is transmitted via light. Multiple FBG sensors can be connected to a single, 250 μm-diameter optical fiber. The FBG optical signal can easily be transmitted over a distance of 10 km and is immune to electromagnetic interference, short circuits or lightning. The stability of optical fiber is not significantly affected by submergence under water. These unique features make FBG sensors ideally suited for the purpose of monitoring ground conditions where profile information is required. The authors have developed an FBG piezometer based on the technique reported by Ho et al. (2008). An array of FBG piezometers can be installed in a single borehole to monitor the profile of the pore-water pressure on a real-time basis. When coupled with the limiting equilibrium or the field stress path framework, as described above, it is possible to establish a landslide warning system based on field h_p profile measurements on a real-time basis.

The field installation of an FBG piezometer array was tested in a highway slope of Alishan Mountain in Southern Taiwan. This paper describes the techniques of FBG pressure sensing and the installation of the FBG piezometer array in a single borehole that was 60 m deep. The h_p profiles recorded during three major typhoons, from 2008 to 2010, a slope stability analysis using the infinite slope, the field stress path and the limiting equilibrium frameworks based on the field h_p data and implications for future applications as part of a landslide warning system are presented and discussed.

2. Partially distributive FBG piezometers

A fiber Bragg grating (FBG) is made by the periodic variation in the core refractive index on a segment of optical fiber 1–20 mm long (Meltz et al., 1989). When the FBG is illuminated by a wideband light source, a fraction of the light is reflected back upon interference by the FBG. The wavelength of the reflected light is linearly related to the longitudinal strains of the FBG. Thus, FBG has the same function as a strain gage. The returned signal from every FBG carries a unique range or domain of wavelength, making it possible to have multiple FBG elements on the same fiber. The multiplexing among various sensors on a single optical fiber can be accomplished by wavelength division addressing, as conceptually described in Fig. 3. There is a limited bandwidth of the light source and, as the light passes an FBG, there is a loss of intensity; the number of FBG sensors that can be placed on a fiber is not more than 20 with the currently available FBG interrogation systems.

Fig. 4 shows a schematic view and photograph of an FBG pressure transducer. The FBG was used to sense the

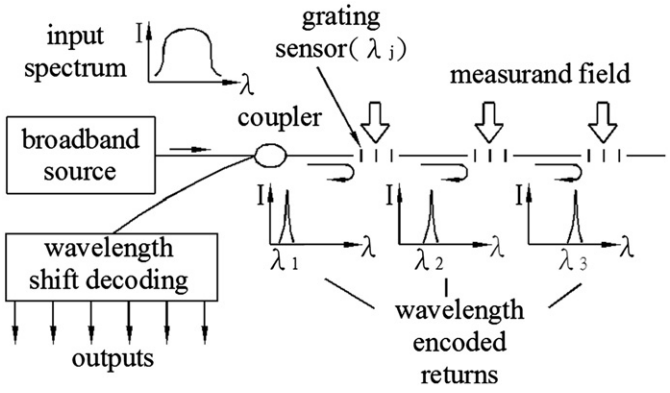

Fig. 3. FBG sensor array (after Kersey, 1992).

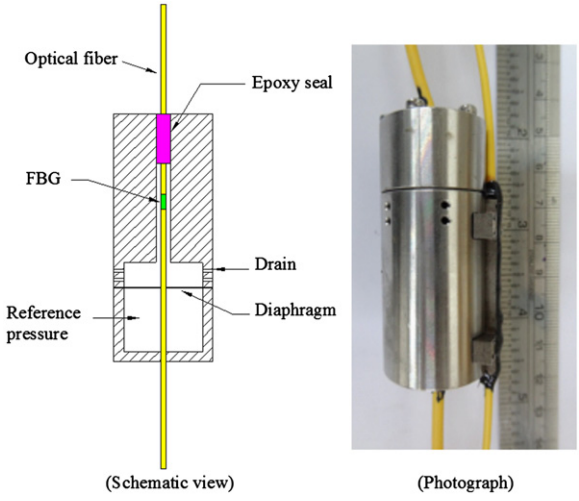

Fig. 4. FBG pressure transducer.

deflection of a metallic diaphragm inside of the transducer due to changes in pressure against the atmosphere. A separate FBG was placed inside the transducer to monitor the fluctuations in temperature. A typical interrogation system is capable of detecting the shifting of the FBG wavelengths by 1 pm (10^{-12} m). An FBG breaks when stretched by a strain equivalent to approximately 8000–10,000 pm in wavelength variation. The range of the pressure transducer was controlled by the stiffness of the diaphragm. Depending on the required safety margin, the maximum allowable pressure was designed to correspond to 1000–6000 pm of the FBG wavelength variation. The completed FBG pressure transducers were calibrated in a sealed chamber. The chamber pressure was controlled pneumatically and monitored with a highly accurate pressure gauge to provide reference readings. The main function of the FBG transducer was to measure positive pressure, although it could also respond to a limited level of negative pressure as in the case of most electronic pressure sensors. Fig. 5 describes the typical results of FBG pressure transducer calibration tests. The calibration covers a pressure range of −50–600 kPa, with a sensitivity of 0.1 kPa (a change in pressure that corresponds

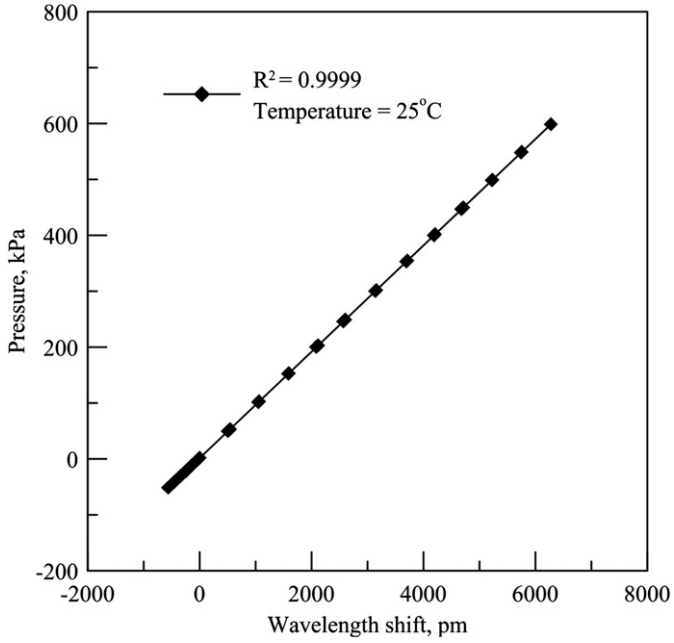

Fig. 5. Results of FBG pressure transducer calibration.

to a 1 pm shifting of the FBG wavelength) and an accuracy of ±0.314% full scale. The negative pressure was applied to the chamber by a vacuum pump and a vacuum pneumatic regulator. The accuracy is defined as

$$\text{Accuracy} = \sqrt{\frac{\sum(\text{measured value} - \text{calibration curve})^2}{(\text{number of measurements} - 1)}} \quad (4)$$

The pressure transducer was converted into a piezometer by surrounding the drains with a non-woven geotextile that served as filter material. With a diameter of 25 mm, the FBG piezometer was fitted inside of a 28 mm ID and 32 mm OD PVC (Polyvinylchloride) pipe. Small drainage holes were drilled in the PVC pipe in areas surrounding the piezometer to allow the passage of water. The piezometer was epoxied and sealed at both ends in the PVC pipe to prevent seepage between piezometers from within the PVC pipe. The PVC pipe serves as a spacer and housing for the piezometers and optical fiber. All PVC pipe connectors were fitted internally so as to leave a smooth exterior upon assembly in the field. The assembled PVC pipe/piezometers can be fully grouted in a borehole following the procedure reported by Contreras et al. (2008). Or, the piezometers can be surrounded by a sand pack and the space between the sand packs sealed with bentonite. A comparison between an array of FBG piezometers installed in a single borehole to the case of the separate, individual installation of standpipes is depicted in Fig. 6. As described above, while the FBG pressure transducer could respond to a limited level of negative pressure, the piezometer was not designed to measure matrix suction. There was no high air entry ceramic filter involved in the piezometers.

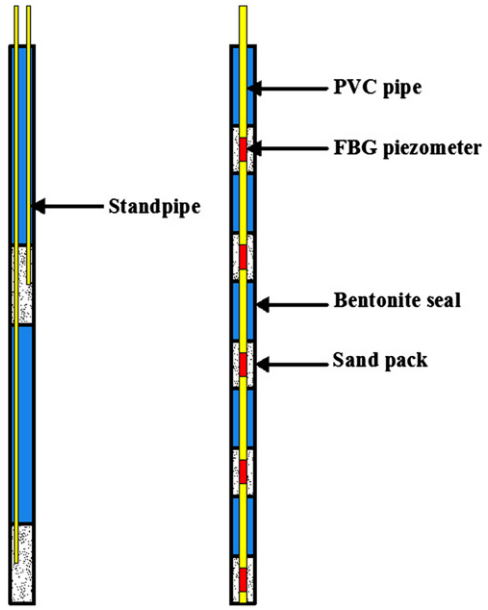

Fig. 6. Comparison between individual separate and piezometer array installations.

3. Field installation at Five Turn Point

A section of Highway 18 that connects Chiayi County to Alishan Mountain, referred to as Five Turn Point, has been selected as the most dangerous highway in Taiwan. Five Turn Point is located in a slope area, of approximately 1200 m × 1000 m, where the ground surface elevation changes by as much as 400 m. Alishan is a major mountain resort in Southern Taiwan that attracts a large number of tourists in the summer, which is also the typhoon season. Fig. 7 presents a topographic map of the general area of Five Turn Point. The highway in this section originally had five turns in order to increase the linear dimension and to maintain a desirable grade for vehicles. At least eight sectors (designated as N1–N8 in Fig. 7) within the Five Turn Point area have been identified with either previous slope failures or signs of continuous movement. The shear planes could reach as much as 80 m below the ground surface. The most recent massive landslide occurred at N4 on June 26, 2003. The slope failure and the rerouting of the highway created additional turns. Fig. 8 depicts the cross sectional view of section B-B that has an average slope angle of 23°. The shear planes associated with earlier ground failures, according to the available investigations, are also included in Fig. 8. Previous subsurface explorations revealed that the subject area was covered by 0–26 m of colluvial material that consisted of a mixture of soil and rock pieces (Land Engineering Consultants, Co., Ltd., 2007). Interlayered sandstone and shale extended from below the colluvial material to over 200 m (the deepest borehole available) below the ground surface. Affected by numerous folding and fault movements, the rock formation was severely fractured with no consistent joint pattern. The

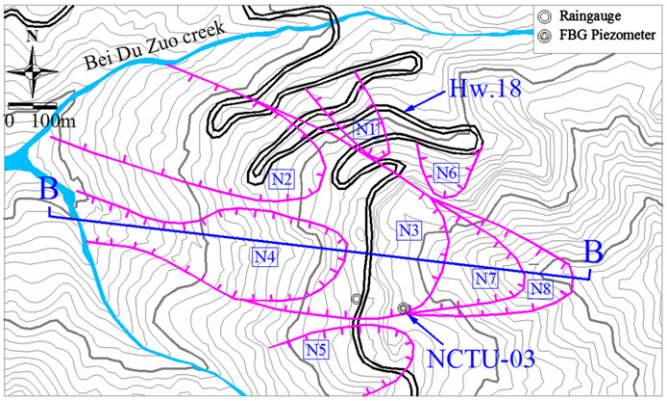

Fig. 7. Topographic map of Five Turn Point (after Land Engineering Consultants, Co., Ltd., 2007).

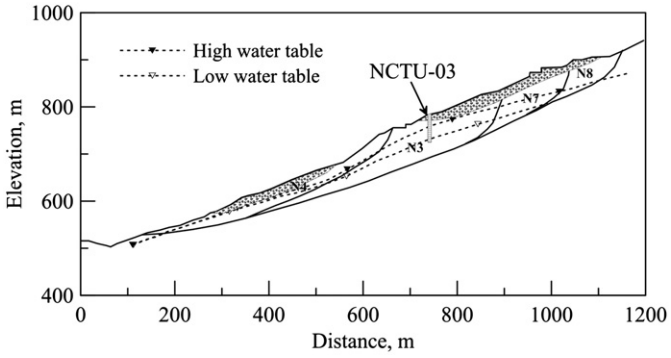

Fig. 8. Section B-B of Five Turn Point (after Land Engineering Consultants, Co., Ltd., 2007).

rock quality designator (RQD), obtained from rock coring, ranged from below 5 to over 50 with no consistent trend with depth. The random RQD values were observed even in boreholes as deep as 200 m. Due to the wide range in sizes of the fractured rock pieces, it was not possible to obtain good quality samples for laboratory shearing tests or to provide representative strength parameters. Open-end piezometers or standpipes, with measuring tips 50–80 m below the ground surface, have been used to monitor the groundwater table. The groundwater rose from its low level by more than 20 m as a result of heavy rainfalls, according to the available data shown in Fig. 8. The sudden and significant changes in the groundwater table are believed to have been a major cause of the earlier slope failures in this area.

A 60-m-deep borehole, marked as NCTU-03 in Figs. 7 and 8, was used to install the FBG piezometer array. The highway section next to NCTU-03 had a mileage mark of 45 km (i.e., 45 km from the starting point of Highway 18 on level ground). The FBG piezometers were housed in PVC pipes as previously described. Additional PVC pipes were connected in the field to space the FBG piezometers at 5 m intervals. The segment of the PVC pipes that contained the FBG piezometers was wrapped with 1.5-m-wide non-woven geotextile outside the PVC pipes as filter.

Fig. 9. PVC pipes and those with FBG piezometers enclosed.

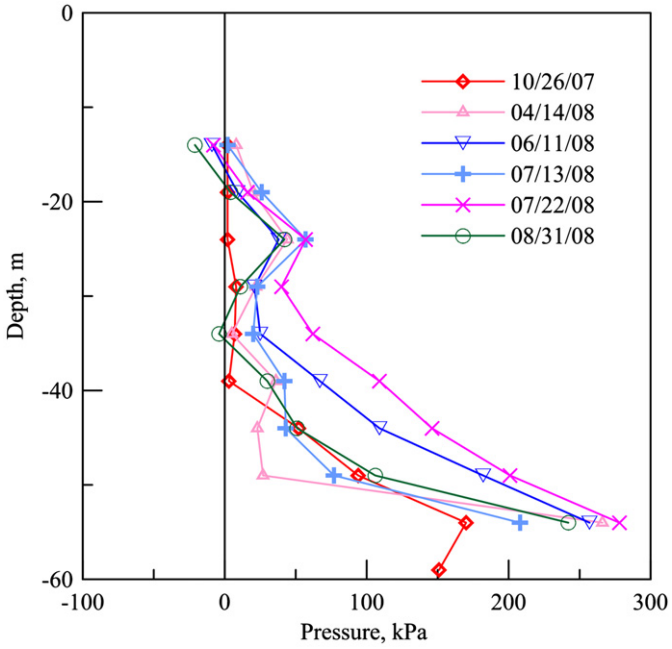

Fig. 10. Piezometer records up to 8/31/2008.

Fig. 9 shows a set of PVC pipes with enclosed FBG piezometers. The optical fibers were threaded through the inside of the PVC pipes. The final assembly was made as each PVC pipe was lowered into the borehole. The borehole had a nominal diameter of 150 mm (6 in.). A steel casing with an inside diameter of 100 mm was extended to the bottom of the borehole before the piezometer installation. The FBG piezometer array was fully assembled and inserted into the borehole with the protection of the steel casing. The steel casing was then lifted upward, 5 m at a time, leaving 5 m of the FBG piezometer array/PVC pipe exposed to the surrounding material. The FBG piezometers were surrounded by 2-m-thick sand packs (see Fig. 6). Sealing between the sand packs was provided by the placing of bentonite pellets. The sand and the bentonite pellets were pumped by water to the desired depth in the borehole using a 32 mm OD PVC pipe as a tremie pipe. The deepest piezometer was located 59 m below the ground surface. The sensors were connected to an on-site computer using optical fiber cables for optical signal interrogation and data logging. The field computer was accessed via the High-Speed Downlink Packet Access (HSDPA) wireless internet system. The readings were updated hourly.

3.1. Field measurements through three typhoons

The FBG piezometer installation at Five Turn Point was completed in mid-October, 2007. Fig. 10 shows a set of representative readings taken between October 26, 2007 (beginning of the automated data logging) and August 31, 2008. The piezometer at 59 m malfunctioned right from the beginning. The initial readings reflected a groundwater table 40 m below the ground surface. The water table remained low for most of the monitored period, as seen in Fig. 10, except for on 6/11 and 7/22 of 2008, when a mild rainstorm occurred. A perched water table developed at 24 m after April 14, 2008. Negative pore-water pressure was registered 14 m below the ground surface in the early stage of monitoring, although the values may not be correct as the piezometers were not equipped with a high air entry ceramic filter.

The Five Turn Point slope has endured three major typhoons since September 2008, and it has remained stable until now (December, 2011). Typhoon Sinlaku landed in Southern Taiwan on September 14, 2008 and brought rainfall that peaked at 660 mm/day with an accumulated value approaching 1000 mm. A histogram of the daily precipitation during the period that includes typhoon Sinlaku is shown in Fig. 11. The rain gauge, with its location marked in Fig. 7, was located within 100 m of the piezometer borehole (NCTU-03 in Figs. 7 and 8). Typhoon Sinlaku was responsible for a bridge collapse at mileage 28.3 km and a mild slope failure at 39 km. Fig. 12 shows a set of representative h_p profiles based on the FBG piezometer readings recorded from the beginning of typhoon Sinlaku to the time when h_p reached the maximum measurement values. The rainfall intensity peaked on September 14, while the maximum h_p profile was recorded on September 15 with a one-day lag. The presentation of h_p profiles followed the same infinite slope framework as in Fig. 1, except that the h_p values were taken from field measurements rather than the one-dimensional seepage analysis. The stability envelopes included in Fig. 12 were determined using Eq. (1). The highly fractured rock pieces were thought to be coarse granular material. The analysis considered the cross section shown in Fig. 8,

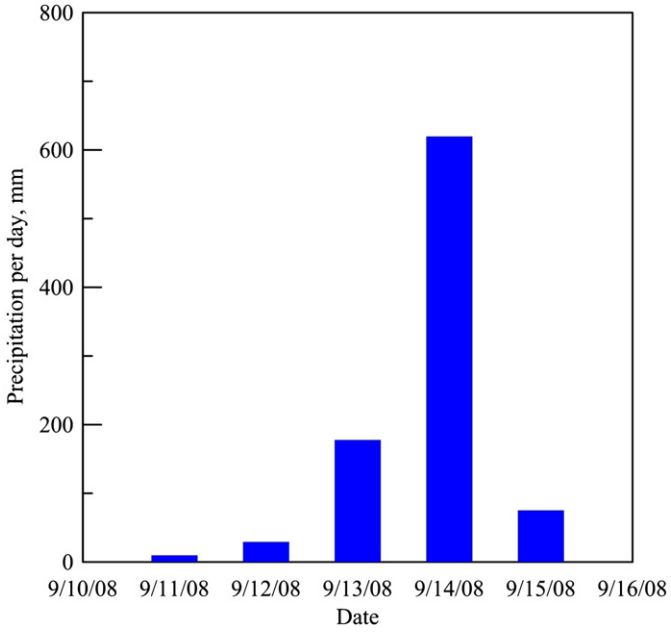

Fig. 11. Rainfall records during typhoon Sinlaku.

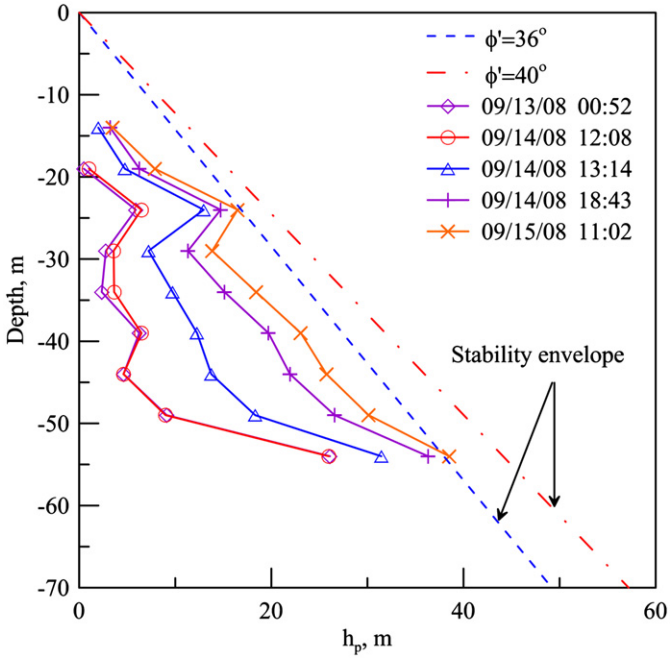

Fig. 12. Profiles of h_p during typhoon Sinlaku.

with a slope angle (β) of 23° and selected ϕ' values, while ϕ^b and c' were assumed to be 0 and $\gamma = 2\gamma_w$. The h_p profiles showed the significant development of a perched water table 24 m below the ground surface. This phenomenon is believed to have been caused by the decrease in hydraulic conductivity at the interface where the ground material changed from a saturated state to an unsaturated state when water seeped into the ground, as described by Collins and Znidarcic (2004) for slopes with coarse material. Fig. 12 also demonstrates that if the ground material had a ϕ' of less than 36°, the slope would have failed with shear planes developing 24 and 54 m below the ground surface.

The pore-water pressure readings also enabled the concept of the field stress path (Anderson and Sitar, 1995; Cascini et al., 2010) to be used in evaluating the stability of the slope. The initial state of stress at each of the pore-water pressure measurement locations was computed using the commercial software SIGMA/W (GEO-SLOPE International Ltd., 2007a). The computation was based on the cross section shown in Fig. 8. The ground material was assumed to be linear elastic with Young's modulus $E = 3310$ MPa, Poisson's ratio $\mu = 0.35$ and $\gamma = 2\gamma_w$. These material parameters were determined considering the laboratory and field geophysical test results reported by Land Engineering Consultants, Co., Ltd. (2007). For simplification, the single γ value used in the computation reflects the saturated state even when the material could be unsaturated. The potential errors from the simplification of the unit weight and the stress–strain relationship are insignificant in comparison to the stress level and the effects of pore-water pressure variations (Anderson and Sitar, 1995). Considering plane strain conditions, p (or p') and q were calculated according to Eqs. (2) and (3), respectively. As the measured pore-water pressure increased, q at a given measurement point remained constant, while p' decreased and the corresponding stress point (p', q) moved laterally towards a failure envelope, as shown in Fig. 13. The (p', q) points depicted in Fig. 13 correspond to the respective points of the nine FBG piezometers installed in the field. The lower left (p', q) points represent the state of field stress at shallower depths. The results also show a potential failure envelope that corresponds to a ϕ'close to 36°. The advantage of the field

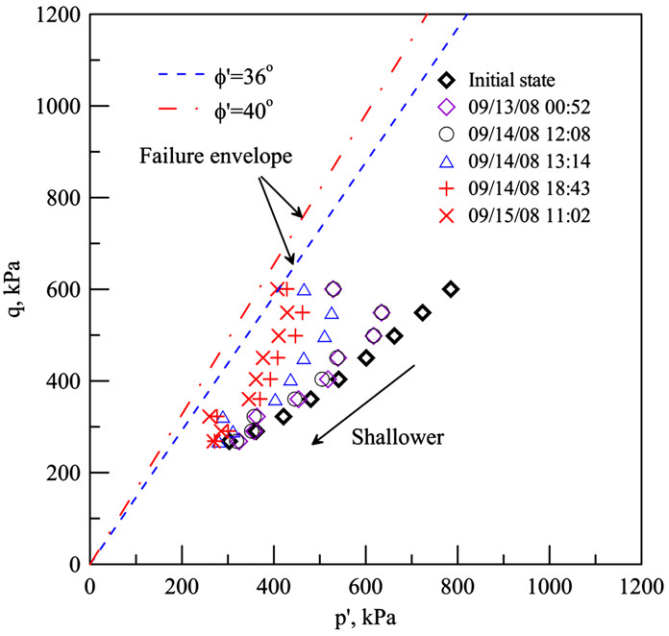

Fig. 13. Evolution of field stress paths during typhoon Sinlaku.

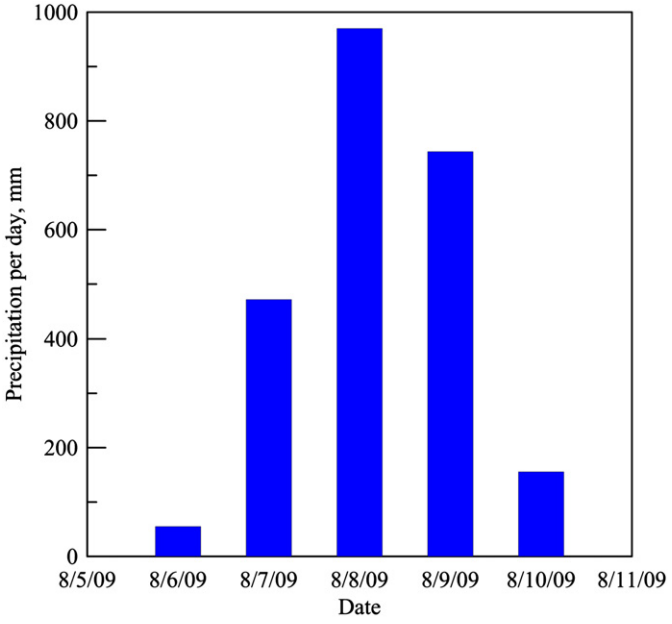

Fig. 14. Rainfall records during typhoon Morakot.

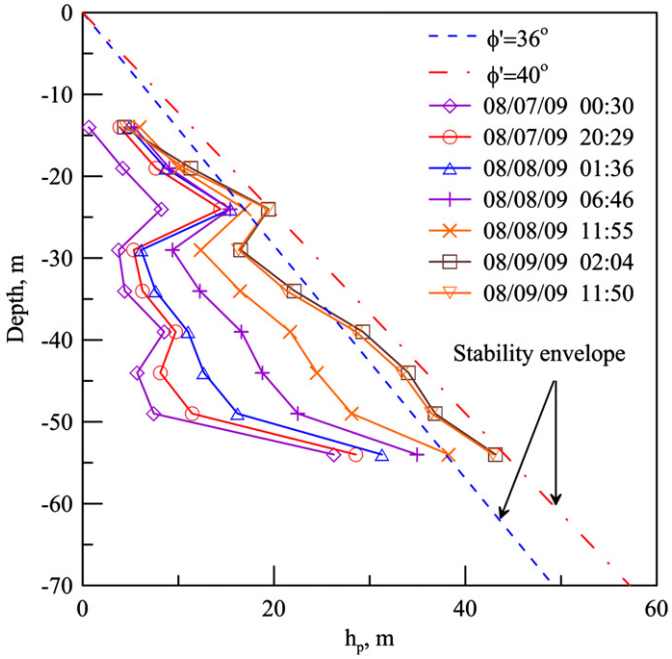

Fig. 15. Profile of h_p during typhoon Morakot.

stress path approach is that it is not necessary to simplify the slope as infinitely long, as in the analysis by Collins and Znidarcic (2004). Although not necessary for the Five Turn Point case, variations in slope angle and ground layers can be readily incorporated into the analysis under the framework of a field stress path. It should be noted that the outcome of the linear elastic stress analysis was not sensitive to the selection of Young's modulus. However, the selection of Poisson's ratio could have significant effects on the initial p, q values.

Typhoon Morakot landed in Southern Taiwan on August 8, 2009. A histogram of the daily precipitation during typhoon Morakot, as shown in Fig. 14, reflects an accumulated rainfall close to 3000 mm. This is more than the average annual rainfall of 2500 mm for all of Taiwan. Rainfall, with an intensity exceeding 700 mm/day, continued through August 9, 2009. Extensive shallow slope failures occurred along Highway 18 at mileage 37.5 km, 40.1 km, 40.7–41.6 km, 54–57.3 km, 59.1 km, 60.7 km, 67.9 km, 71 km and 79 km. Of these points, the slope failure at 59.1 km was the most significant as it covered an area of 50 ha. Unlike typhoon Sinlaku, the measured pore-water pressure at NCTU-03 did not show a delayed development; the peak values were reached soon after the rainfall started subsiding on August 9. The most significant increase in pore-water pressure occurred at depths between 30 and 50 m. The intense rainfall is also believed to have induced a perched water table 24 m below the ground surface, as in the case of typhoon Sinlaku. Using the same slope angle, material properties and the stability envelope as those shown in Fig. 12 for typhoon Sinlaku, slope failure could be predicted if the ground material had a $\phi'$of less than 40°, with shear planes 24 and 54 m below the ground surface, as demonstrated in Fig. 15.

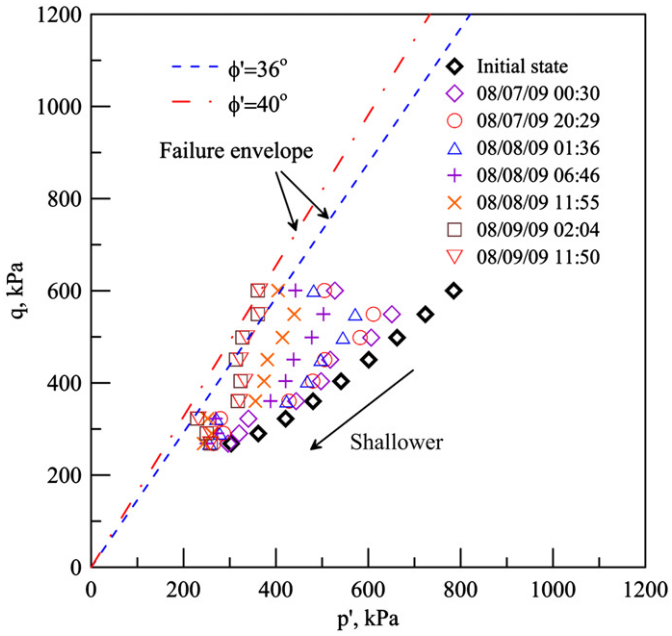

Fig. 16. Evolution of field stress paths during typhoon Morakot.

The evolution of field stress paths for the case of typhoon Morakot are shown in Fig. 16. Consistent with the infinite slope approach, the field stress path analysis also indicated stress points touching the failure envelope that correspond to a ϕ' of 40°.

The rainfall during typhoon Fanapi was concentrated mainly on September 19, 2010, as shown in Fig. 17. With a total amount of less than 300 mm, the rainfall was relatively light. The typhoon caused mild slope failures at mileage 59.3 and 77 km along Highway 18. There was no

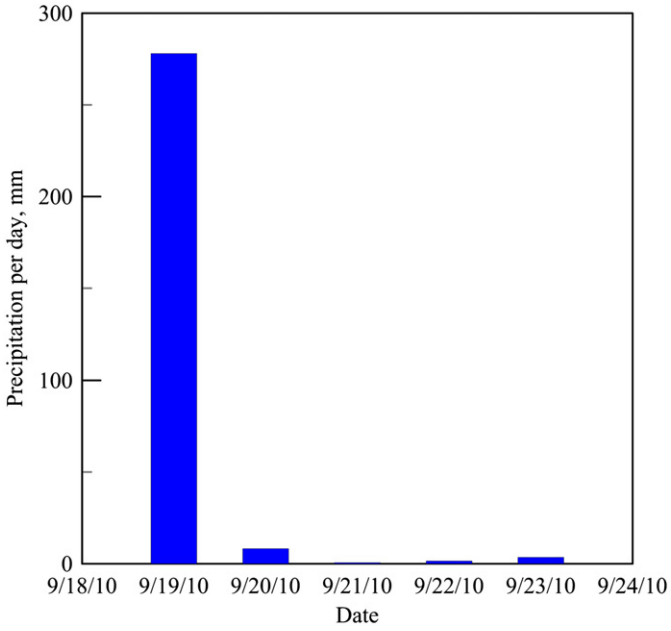

Fig. 17. Rainfall records during typhoon Fanapi.

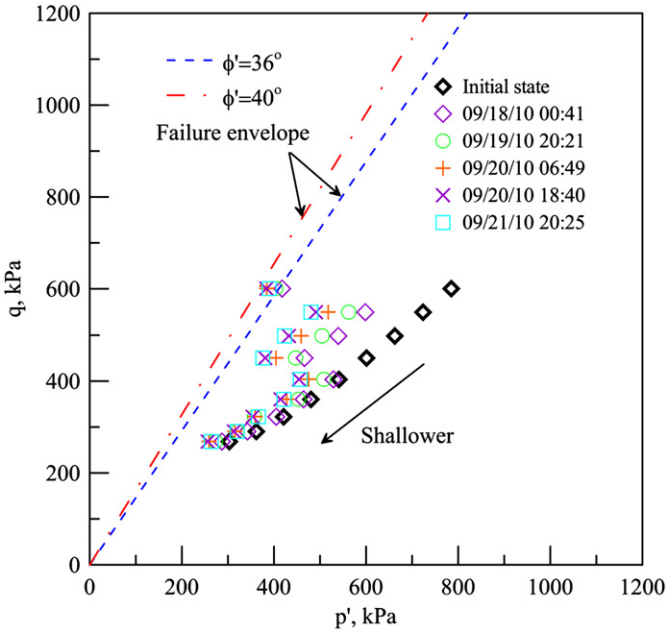

Fig. 19. Evolution of field stress paths during typhoon Fanapi.

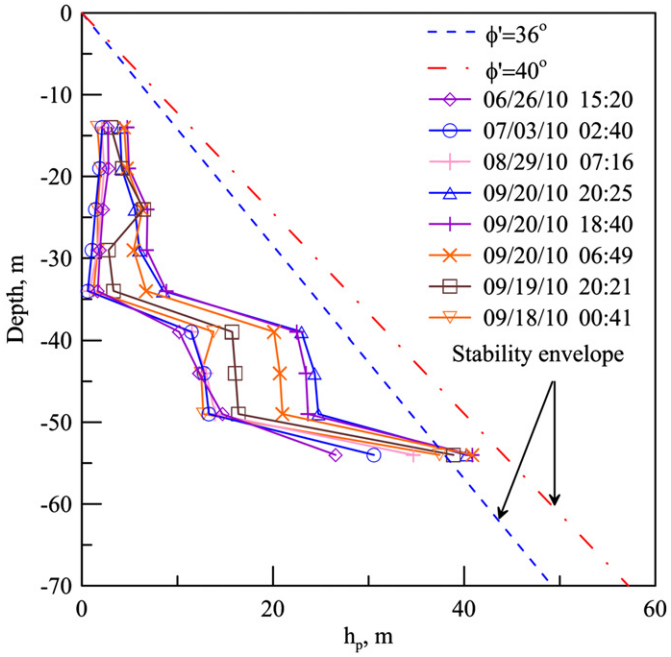

Fig. 18. Profiles of h_p during typhoon Fanapi.

clear sign of perched ground water at shallow depths according to the FBG piezometer readings. Most of the pore-water pressure that increased during typhoon Fanapi occurred at depths between 40 and 50 m. Unlike the past two typhoons, the relatively high pressure head at the depth of 54 m was high before the typhoon and continued to increase towards the end of the typhoon, as described in Fig. 18. This early and significant development of pressure head at 54 m may be associated with the influx of spring water or seepage from the upper parts of the slope. Due to these initial conditions, the slope was in a more critical condition than at the time of typhoon Sinlaku when the rainfall was much more intense. Both the infinite slope (Fig. 18) and the field stress path (Fig. 19) approaches indicated that it would require a ϕ' of more than 36° to maintain the slope stability. Regardless of the rainfall characteristics during the above-reported typhoons, none of the field measurements reflected a pore-water pressure profile that is similar to the hydrostatic one.

A series of slope stability analyses was also performed for the same cross section shown in Fig. 8 using the conventional method of slices. The analysis was conducted using the commercial software SLOPE/W (GEO-SLOPE International Ltd., 2007b), considering the circular failure surfaces under the Bishop method. The pore-water pressure head profile, taken from the peak values during each of the three typhoons, was used. These values are shown in Table 1; linear interpolation was used for the pore-water pressure between the piezometers. The analysis assumes the same variation in pore-water pressure with depth for the entire slope. The factors of safety reported in Table 2, from the method of slices, are generally lower, but show a similar trend to those from the infinitely long slope and field stress path methods.

It should be emphasized that there was no apparent sign of slope failure in the areas immediately surrounding borehole NCTU-03 throughout the above-mentioned three typhoon seasons.

4. Concluding remarks

The FBG piezometer array, installed at Five Turn Point over four years ago, continues to work today (April, 2012). Nine piezometers, spaced at 5 m intervals, were installed in

Table 1
Pressure head profiles used in the method of slice analysis.

Typhoon	Depth									
	0 m	14 m	19 m	24 m	29 m	34 m	39 m	44 m	49 m	54 m
Sinlaku	0	3.46	7.81	16.42	13.78	18.35	22.96	25.64	30.03	38.45
Morakot	0	4.53	10.55	19.3	16.24	21.15	28.38	33.15	36.29	42.79
Fanapi	0	3.25	3.4	3.99	4.69	7.16	22.79	24.41	25.18	42.4

Table 2
Factors of safety from the analysis using the method of slices.

Friction angle	Typhoon		
	Sinlaku	Morakot	Fanapi
36°	0.97	0.92	0.80
40°	1.12	1.07	0.92
45°	1.34	1.27	1.09

a single borehole with depths ranging from 14 to 54 m below the ground surface. The system performed well through three major typhoons during this period. The stability and durability are mainly due to the unique properties of the optical FBG sensing systems. The experience shows that with the help of partially distributive sensors, field pore-water pressure profile monitoring can be practically implemented. Based on the data collected through the three typhoons, the following conclusions can be drawn:

- The pore-water pressure readings obtained at the test site before and during a typhoon deviate significantly from the linear hydrostatic distribution. To properly reflect the hydrological conditions, it is imperative to measure the pore-water pressure profile, especially in the case of a potentially deep-seated slope failure.
- Depending on the nature of the rainfall pattern and the groundwater flow, the buildup of pore-water pressure may show different characteristics. The local rainfall may not be the major factor in controlling the stability of a slope.
- By coupling the automated pore-water pressure profile measurements with the infinite slope or field stress path concept, it is feasible to establish a real-time slope failure warning system that is based on the proximity between the stress state and a stability envelope. This mechanics-based warning system should be preferable to the empirical methods that use ground displacement measurements or rainfall as the key parameters.

The FBG piezometer array enables pore-water pressure profile measurements to be made at a selected location, along the borehole direction. The monitoring may not be effective unless the selected location represents the most critical position in a slope. Also, the friction angles used in this paper were selected rather than measured. An effective scheme to determine the strength parameters for deep-seated fractured rock pieces or earth material that involve large particle sizes is necessary for establishing a priori failure envelope as part of the landslide warning system.

Acknowledgments

The research described in this paper has been funded by the National Science Council of Taiwan under Contract nos. 97-2625-M-009-009, 97-2625-M-211-001, 98-2625-M-009-003-MY2, and 100-2625-M-009-005-MY3, Harbor and Marine Technology Center, Water Resources Agency and Chunghwa Telecom Co. The support is gratefully acknowledged.

References

Anderson, S.A., Sitar, N., 1995. Analysis of rainfall-induced debris flows. ASC Journal of Geotechnical Engineering 121 (7), 544–552.

Cannon, S.J., Ellen, S.D., 1985. Rainfall conditions for abundant debris avalanches, San Francisco Bay region, California. California Geology 38 (12), 267–272.

Cascini, L., Cuomo, S., Pastor, M., Sorbino, G., 2010. Modeling of rainfall-induced shallow landslides of the flow-type. Journal of Geotechnical and Geoenvironmental Engineering 136 (1), 85–98.

Cowland, J.W., Richards, L.R., 1985. Transient groundwater rises in sheeting joints in a Hong Kong granite slope. Hong Kong Engineer, 27–32.

Collins, B.D., Znidarcic, D., 2004. Stability analyses of rainfall induced landslides. Journal of Geotechnical and Geoenvironmental Engineering 130 (4), 362–372.

Contreras, I.A., Grosser, A.T., Ver Strate, R.H., 2008. The use of the fully grouted method for piezometer installation. Geotechnical Instrumentation News 26, 30–37 June.

De Vita, P., Reichenbach, P., 1998. Rainfall-triggered landslides: a reference list. Environmental Geology 35 (2–3), 219–233.

Fannin, R.J., Jaakkola, J., 1999. Hydrological response of hillslope soils above a debris-slide headscarp. Canadian Geotechnical Journal 36, 1111–1122.

GEO-SLOPE International Ltd., 2007a. SIGMA/W for Stress-deformation. Version 7.17, User's Guide. Geoslope Int. Lad., Calgary, Alta., Canada.

GEO-SLOPE International Ltd., 2007b. SLOPE/W for Slope Analysis. Version 7.17, User's Guide. Geoslope Int. Lad., Calgary, Alta., Canada.

Ho, Y.T., Huang, A.B., Lee, J.T., 2008. Development of a chirped/differential optical fiber Bragg grating pressure sensor. Journal of Measurement Science and Technology 19, 6. http://dx.doi.org/10.1088/0957-0233/19/4/045304.

Johnson, K.A., Sitar, N., 1990. Hydrologic conditions leading to debris-flow initiation. Canadian Geotechnical Journal 27, 789–801.

Keefer, D.K., Wilson, R.C., Mark, R.K., Brabb, E.E., Brown, W.M., Ellen, S.D., Harp, E.L., Wieczorek, G.F., Alger, C.S., Zatkih, R.S., 1987. Real-time landslide warning during heavy rainfall. Science 238, 921–925.

Kersey, A.D., 1992. Multiplexed Fiber Optic Sensors. In: Fiber Optic Sensors, Proceedings of SPIE, vol. CR44, pp. 200–225.

Kitamura, R., Sako, K., 2010. Contribution of "Soil and Foundations" to studies on rainfall-induced slope failures. Soil and Foundations 50m (6), 955–964.

Land Engineering Consultants, Co., Ltd., 2007. Highway 28.9 km–31.5 km (Five Turn Point) Landslide Investigation, Remediation Planning and Safety Evaluation. 3rd Overall Report. Department of Highway Maintenance, Section V (in Chinese).

Meltz, G., Morey, W.W., Glenn, W.H., 1989. Formation of Bragg gratings in optical fibers by a transverse holographic methods. Optics Letters 14, 283.

Ng, C.W.W., Zhan, L.T., Bao, C.G., Fredlund, D.G., Gong, B.W., 2003. Performance of an unsaturated expansive soil slope subjected to artificial rainfall infiltration. Géotechnique 53 (2), 143–157.

Ng, C.W.W., Springman, S.M., Alonso, E.E., 2008. Monitoring the performance of unsaturated soil slopes. Geotechnical and Geological Engineering 26 (6), 799–816.

Rahardjo, H., Nio, A.S., Leong, E.C., N.Y., Ng Yew Song, 2010. Effects of groundwater table position and soil properties on stability of slope during rainfall. Journal of Geotechnical and Geoenvironmental Engineering 136 (11), 1555–1564.

Sidle, R.C., 1984. Shallow groundwater fluctuations in unstable hillslopes of Coastal Alaska. Zeitschrift für Gletscherkunde und Glazialgeologie 20, 79–95.

Zhan, L.T., Ng, C.W.W., Fredlund, D.G., 2007. Field study of rainfall infiltration into a grassed unsaturated expansive soil slope. Canadian Geotechnical Journal 44, 392–408.